

# On the dynamics of rotating machinery supported by AMB during base motion

Clément JARROUX\*, Jarir MAHFOUD\*, Régis DUFOUR\*, Benjamin DEFOY\*\* and Thomas ALBAN\*\*

\*Université de Lyon, INSA-Lyon, LaMCoS UMR5259

18-20 rue des Sciences, Bât J. d'Alembert, 69621 Villeurbanne Cedex, France

E-mail: clement.jarroux@insa-lyon.fr

\*\*GE Oil & Gas Thermodyn

480 allée G. Eiffel, BP 119, 71203 Le Creusot Cedex, France

## Abstract

This study is devoted to rotor supported by Active Magnetic Bearings (AMBs) and subject to base motion. The machine casing is considered rigid and able to move along the 3 translations and the 3 rotations. The objective of this work is to assess the suitability of machine supported by AMBs to withstand base motions for applications such as compressors on FPSO (Floating production storage and offloading) or emergency steam turbines in nuclear plants. The model developed takes into account the base motion, unbalances on rotor, gravity and bearings properties. The consideration of the base motions has a significant impact on equations of motion and introduces parametric excitations. The centrifugal stiffening effect due to the base rotations is considered. The developed model, is compared with previous experiments performed with a light rotor mounted on classical ball-bearings. The dynamic behavior is analyzed for different types of base motion. Then, the capability of AMB to sustain base motions is examined. Numerical simulations are performed with a rigid rotor supported by two AMBs. The latter are controlled with an augmented PID not specifically tuned for base motion purpose. Finally, the results are discussed. The model developed is a first step for the improvement of turbomachinery supported by AMB. The aim is to eliminate a blocking point to the penetration of AMB technology in on board applications.

**Keywords** : rotor dynamics, active control, active magnetic bearings, base motion, parametric excitations

## 1. Introduction

Nowadays, energy needs in production and transport continue to grow in our modern society and manufacturers must constantly face new technical challenges. Turbomachines manage the fluid-structures energy transfer, therefore they play a vital role and have to be able to withstand severe environmental conditions. Consequently, a major focus of the research engaged by industrials and academic laboratories concerns their reliability in any circumstances. Most of the rotating machinery can be considered as on-board machines. Aircraft engines, automotive turbochargers or compressors fixed on an oil offshore-platform are notable examples. The base motion generates complex rotor dynamics in particular in the case of base rotations yielding parametric instabilities. At certain rotating frequencies of the support, combined with the natural frequencies of the rotor, instability zones emerge and depend on the amplitude of the rotation angle (Dakel et al. 2014a; Dakel et al. 2014b; Duchemin et al. 2006; Han and Chu 2015). The dynamic behavior of on-board rotating machines should then be carefully analyzed to improve the reliability of numerical predictions and to maintain a maximal operability of the machines.

On the other hand, Active Magnetic Bearings (AMBs) are more and more utilized in industrial applications for their different advantages (no wear due to friction, no oil system, compact space requirement...). They are inherently unstable, therefore a feedback control is needed and the PID is the most implemented controller. Some studies focused on the control of rotors subject to base motion using magnetic forces. Rotor vibration control subject to earthquake was first studied in the end of the 1980s by (Murai et al. 1989). The sinusoidal base motion of a non-rotating mass mounted on magnetic bearings was experimentally and numerically analyzed by (Kasarda et al. 2000). Three PID controllers were tested and non-linear responses were found in the less damped controller. The feedforward control loop is often used to control base motion in parallel with a feedback control loop. This method was employed by (Marx and Nataraj 2007) to

reduce the harmonic translation motion of the base considering a rigid rotor supported by non-linear AMBs. This strategy was also used by (Matsushita et al. 2001) to sustain a flexible rotor subject to earthquakes and results are promising. A proportional gain is added to counteract base motion in the feedforward loop while (Suzuki 1998) used the Finite Impulse Filter instead. Three controllers were tested in (Cole et al. 1998) and the  $H_\infty$  controller has the greatest effect in reducing the rotor response due to unbalance and horizontal shock of the base. The wavelet transform combined with the  $H_\infty$  controller led to the best performance in terms of transmitted forces and vibration amplitudes, according to (Keogh et al. 2006).

These studies dealt only with translation motions, as second member in the equations of motion (EoM), where an acceleration vector is multiplied by the rotor mass matrix. To the best of authors' knowledge, no papers consider the energetic method used in (Dakel et al. 2014a; Dakel et al. 2014b; Duchemin et al. 2006) including base rotations and translations, coupled with AMBs. Even if a magnetic actuator was employed by (Das et al. 2010) to deteriorate the instability zones generated by harmonic pitching motions, the rotor was supported by classical bearings.

This energetic method coupled with AMBs is considered here. First, the paper deals with the rigid base motion intakes in the EoM of a finite element rotor model. The developed numerical model is validated with previous experimentations that considered constant stiffness and damping bearings, which then incorporate AMBs with a PID controller. Several types of base motion are imposed; harmonic rotations (pitching and rolling), earthquake and half-sine shock. Results are analyzed in terms of time history rotor deflections and orbits. This work is a part of a research program for the reliable prediction of the dynamic behavior of turbomachinery supported by AMB submitted to their external environment.

## 2. Base motion numerical model

### 2.1 Equations of motion

In classical rotor dynamics analysis, kinetic  $T$  and strain  $U$  energies of each rotor elements as well as the virtual work of external forces  $F_{q_i}$  are set-up to derive the EoM of the system through the Lagrange's equation:

$$\frac{d}{dt} \left( \frac{\partial T}{\partial \dot{q}_i} \right) - \frac{\partial T}{\partial q_i} + \frac{\partial U}{\partial q_i} = F_{q_i} \quad (1)$$

where  $F_{q_i}$  is the external force applied to DOF  $q_i$  of the system. When the rotor support is at rest, equations are well known. The base motion changes deeply the expression of these energies and the EoM of the system. The method chosen here to develop energies comes from (Dakel et al. 2014a; Dakel et al. 2014b; Duchemin et al. 2006). It consists in describing the motion of the rotor with respect to the rigid support, as usually done in classical rotor dynamics, and the support motion with respect to the ground. An intermediate frame describes the energies to investigate the deflection of the neutral line of the rotor in the frame attached to the rigid support. Three Cartesian frames are then defined, as shown in Fig. 1. The Galilean frame of reference  $R^g(x^g, y^g, z^g)$  is attached to the ground, the non-inertial frame  $R(x, y, z)$  to the rigid support and the local non-inertial frame  $R^l(x^l, y^l, z^l)$  to the shaft deflection line.

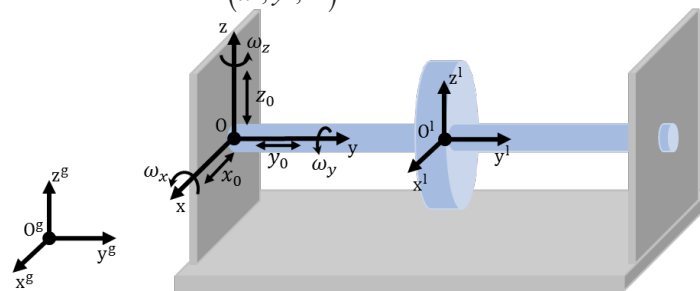


Fig. 1 Frames of reference

The angular velocity vector  $\vec{\omega}_R^{R^g}$  and position vector  $\vec{O^g O}$  describing the base motion with respect to the ground are expressed in the frame attached to the rigid support as follows:

$$\begin{matrix} \overrightarrow{\omega}_R^{R^g} \\ \omega^y \\ \omega^z \end{matrix} = \begin{matrix} \omega^x \\ \omega^y \\ \omega^z \end{matrix} \Big|_R \quad \overrightarrow{O^g O} = \begin{matrix} x_0 \\ y_0 \\ z_0 \end{matrix} \Big|_R \quad (2)$$

The expression of these vectors is detailed in (Dakel et al. 2014a; Dakel et al. 2014b) as well as the kinetic and strain energies of the shaft elements, the kinetic energy of the discs and discrete unbalances and the virtual work of bearing external forces.

The finite element method is used to predict the rotor lateral deflections. Disk and shaft are assumed to be symmetric, the disk rigid and the speed of rotation constant. The shaft is modeled with Timoshenko beam elements with two nodes with four DOF per node. The virtual work of the bearing restoring forces is not affected by the base motion since the base motion is expressed in the rigid support frame. Finally, the equations of the motion have the following expression:

$$M\ddot{\delta} + (\Omega C^g + \omega^y C^{\omega^y})\dot{\delta} + (K^e + \dot{\omega}^y K^{\dot{\omega}^y} + \Omega \omega^y K^{\Omega \omega^y} + \omega^{x2} K^{\omega^{x2}} + \omega^{y2} K^{\omega^{y2}} + \omega^{z2} K^{\omega^{z2}} + \omega^x \omega^z K^{\omega^x \omega^z})\delta = f_{unb} + f_{ext} \quad (3)$$

with  $K^e$  the matrix,  $C^g$  the gyroscopic matrices present in classical rotor dynamics study. All the other matrices depend on the base motion: the second gyroscopic matrix  $C^{\omega^y}$  on the rotating speed  $\omega^y$  of the support along the direction of the shaft line, the stiffness matrix  $K^{\dot{\omega}^y}$  on the rotating acceleration  $\dot{\omega}^y$ , the other stiffness matrices on the square of the angular velocities of the support or on particular combinations. They can be seen as centrifugal effect matrices where the associated stiffening effect is considered. Consequently, the support rotations introduce time-varying parametric excitations able to generate lateral instabilities. The base motion also impacts the mass unbalance forces  $f_{unb}$ . The external forces  $f_{ext}$  contains all the contribution of the translation motions of the support combined with its rotations. For practical reasons, the time dependent / parametric matrices are considered as external forces and placed in the second member of Eq. 3.

## 2.2 Validation of the numerical tool

In order to validate the numerical model, a comparison with previous works is carried out. In (Driot et al. 2006; Duchemin 2003; Duchemin et al. 2006), the rotor, Fig. 2, consists in a shaft of length  $l$  with a circular section of radius  $r_1$ .

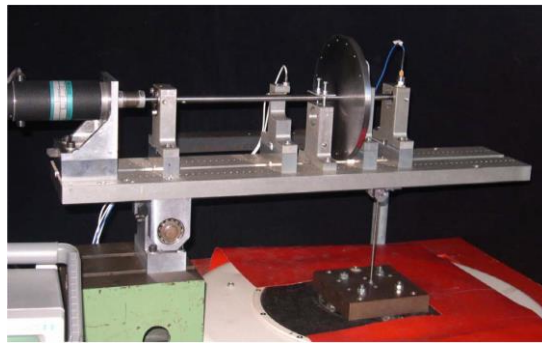


Fig. 2. Picture of the on-board rotor

A rigid disk of thickness  $h$  is placed at the location  $l_d$ . The rotor is mounted on anisotropic bearings having stiffness  $k_{xx}, k_{zz}$  and damping  $c_{xx}, c_{zz}$  coefficients. Table 1 gathers the numerical data. The vertical and horizontal deflections of the shaft are measured with eddy currents sensors located at the middle of the shaft.

Table 1. Rotor properties

$l$ [m]	$r_1$ [m]	$r_2$ [m]	$h$ [m]	$E$ [Pa]	$\rho$ [Kg/m <sup>3</sup> ]	$l_d$ [m]	$k_{xx}$ [N/m]	$k_{zz}$ [N/m]	$c_{xx} = c_{zz}$ [N.s/m]	$r_u$ [m]
0.4	0.005	0.1	0.01	$2.05e^{11}$	7 800	0.3	$2.1e^5$	$1.2e^6$	$15\ 000/\Omega$	0.1

The shaft is discretized into eight beam finite elements of equal length in which the centrifugal stiffening effects due to base rotations are taken into account. Using the modal method reduces the model to the first 12 modes and introduces a modal damping matrix established with a 0.005 viscous damping factor. The responses are predicted with the classical 5th order Runge-Kutta scheme with variable time step. First, the study concerns the case where the shaft runs at a constant speed of rotation  $\Omega = 1\,200$  rpm, below the first flexion mode, with a 160 g.mm unbalance mass  $m_u r_u$  located on the disk at a position  $r_u$  from the center of the shaft line. Rotor was previously balanced, and the residual unbalance is neglected. Then,  $m_u r_u$  is the added unbalance. The base ensures a sinusoidal rotation  $\omega_x$  along the x-axis where the amplitude  $\omega_0 = 1.6e^{-5}$  rad and the frequency  $\Omega_x = 60$  Hz. Figures 3 and 4 compare the measured and predicted deflections.

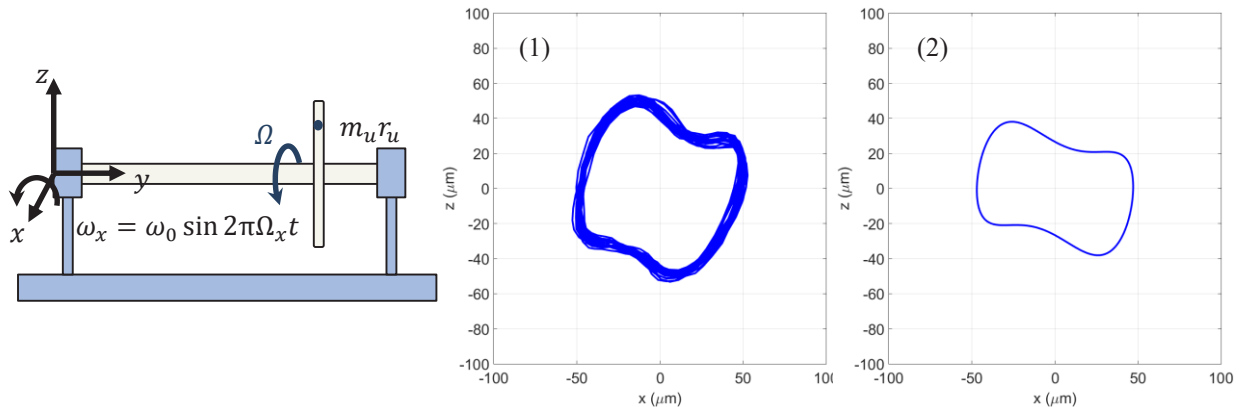


Fig. 3.  $\Omega = 1\,200$  rpm / 60 Hz angular frequency of the base / (1): experiments / (2): numerical simulation

The predicted and measured orbits, Fig. 3, are really close in term of shapes and amplitudes. Orbits are periodic since there is a mathematical relationship between the rotor rotational speed and the harmonic pitching frequency, as explained by (Driot et al. 2006). Transient simulations and tests were also performed, in particular, with a rotation shock of the support. The study concerns the case where the shaft runs at 600 rpm with a 1 030 g.mm unbalance mass  $m_u r_u$ . When the periodic motion is reached, a rotation shock  $\omega_x$  is introduced to the base along the x-axis of maximum amplitude 0.015 radians during 0.5 s, plotted Fig. 4:

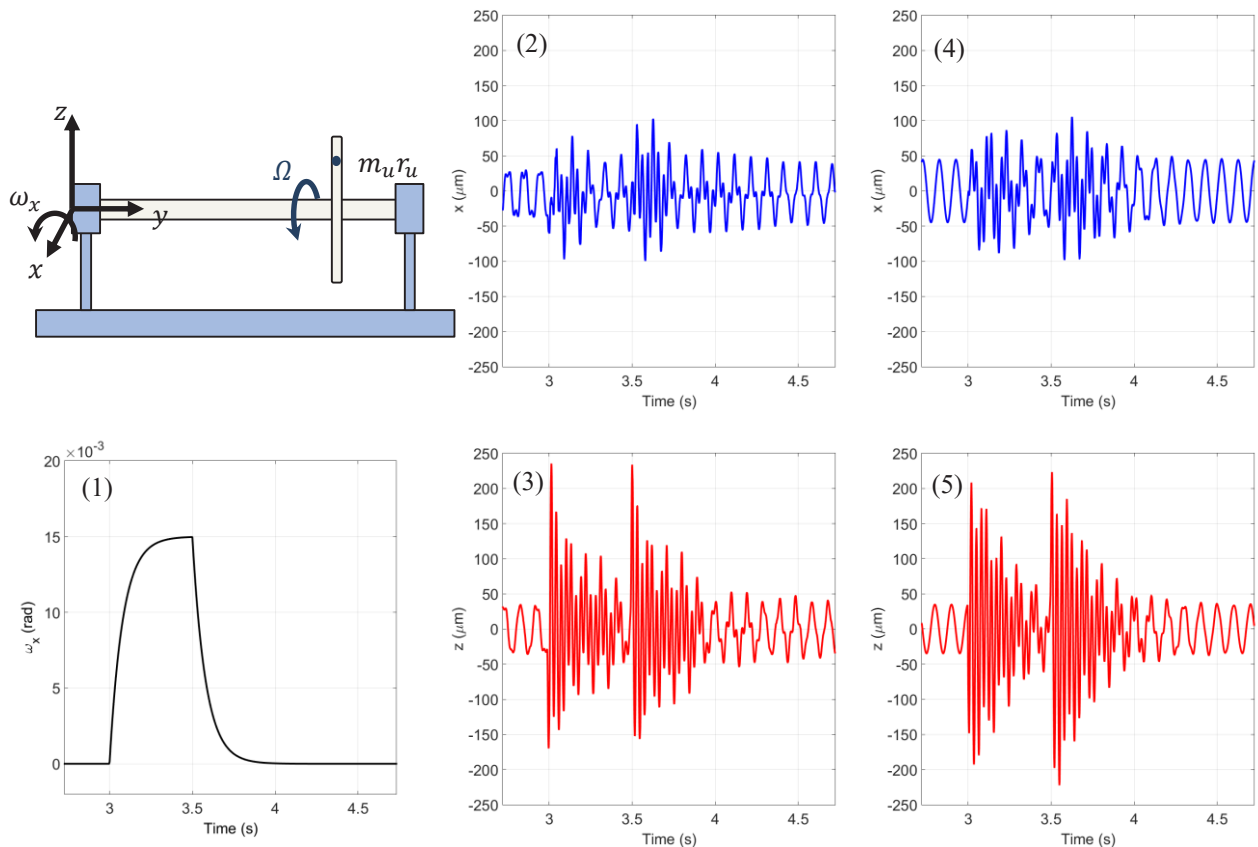


Fig. 4.  $\Omega = 600$  rpm / (1): rotation shock of the base / (2) and (3): experiments / (4) and (5): numerical simulations

The rotor deflections, plotted in Fig. 4, are maximal in the z-direction since the angular shock is applied along the x-axis. These deflections are related to the changes of slope of  $\omega_x$  which correspond to the maximal accelerations. The gyroscopic effects are high on this rotor and coupling between x and z direction is observed. Thus, the horizontal direction is also impacted by this angular impact. Predicted and measured harmonic and impulse responses are in good agreement: the model is able to predict accurately the dynamic phenomena. The model is valid for bearings with constant characteristics. The next part concerns the implementation of AMBs and the numerical assessment of the model.

### 3. Rotor on AMB subject to base motion

#### 3.1 AMB design

Let the rotor supported by AMBs and subject to unbalance forces, gravity and base motion effects. The rotor is based on previous works carried out by (Defoy et al. 2014; Defoy et al. 2015) to investigate the rotor dynamics on AMBs. In the present study, the central shaft diameter has been increased and the disk was decentered in order to obtain the dynamic behavior of a high speed turbomachinery with rigid shaft. The rotor mass and length are respectively 6.5 Kg and 0.65 m. Figure 5 shows the FE mesh and the related normalized eigen vectors. Vibration nodes are present at the non-driving end (NDE) for both the 3<sup>rd</sup> and the 4<sup>th</sup> modes between the sensor and the actuator represented by red point Fig .5. This has to be taken into account for the design of the controller.

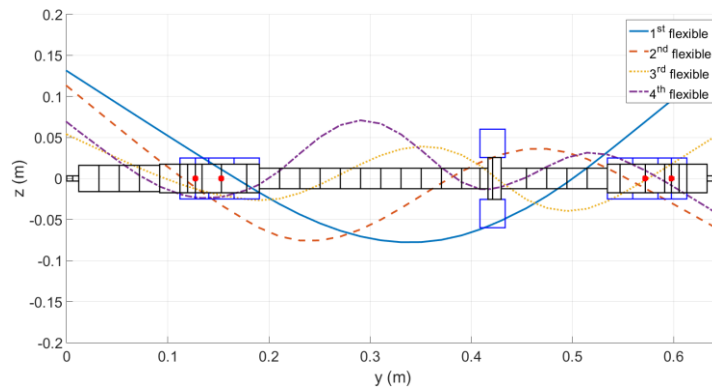


Fig. 5. Rotor model and Eigen mode shapes

Table 2. Rotor natural frequencies

Modes	0 rpm [Hz]	15 000 rpm (backward) [Hz]	15 000 rpm (forward) [Hz]
Rigid 1	75	75	75
Rigid 2	92	89	94
1	203	194	213
2	581	563	598
3	1 142	1 036	1 260
4	2 103	2 088	2 119

Results summarized in Table 2 show that the rotor remains rigid when running at 9 500 rpm (158 Hz). The calculation of the natural frequencies were performed with a direct stiffness ( $8e^5 \text{ N.m}^{-1}$ ) representative of the magnetic bearing stiffness characteristics. The AMBs, represented by the restoring force  $f_{amb}$ , have a static load capacity of 280 N each. They are powered in differential driving mode with a bias current  $I_0$  equals to 1 A and a control current  $i$  as shown in Eq. 4. Currents are provided in the range of  $0-3A$ .

$$f_{amb} = 4\xi_B \mu_0 S N^2 \left[ \frac{(I_0 - i)^2}{\left(2g_0 - 2x + \frac{L}{\mu_r}\right)^2} - \frac{(I_0 + i)^2}{\left(2g_0 + 2x + \frac{L}{\mu_r}\right)^2} \right] \quad (4)$$

With  $\xi_B$  a parameter depending on the bearing geometry (0.92 in this case),  $\mu_0$  the magnetic permeability of the vacuum,  $S$  the pole area and  $N$  the number of turns in one coil,  $g_0$  the nominal air gap (432  $\mu\text{m}$ ),  $x$  the rotor position,  $\mu_r$  the relative permeability of iron core and  $L$  the average length of the magnetic flux lines. The magnetic force  $f_{amb}$  is linearized in the range of operating position since the AMBs are powered in differential driving mode, as shown in Eq. 5. This assumption remain valid for rotor deflections leading to contact with TDB (100  $\mu\text{m}$ ). Current saturation effects are not taken into account.

$$\left. \begin{aligned} K_i &= \left. \frac{\partial f_{amb}}{\partial i} \right|_{\substack{x=0 \\ i=I_w}} = \frac{-16\xi_B\mu_0SN^2I_0}{\left(2g_0 + \frac{L}{\mu_r}\right)^2} \\ K_x &= -\left. \frac{\partial f_{amb}}{\partial x} \right|_{\substack{x=0 \\ i=I_w}} = \frac{-32\xi_B\mu_0SN^2(I_0^2 + I_w^2)}{\left(2g_0 + \frac{L}{\mu_r}\right)^3} \end{aligned} \right\} \Rightarrow f_{amb} \cong K_i i - K_x x \quad (5)$$

The negative stiffness  $K_x$  is a consequence of the attractive forces produced by the electromagnets when they are supplied with constant current while the current stiffness  $K_i$  comes from the stiffening effect of the current control. The electronic part of the AMBs is taken into account with a first order low pass filter with a 2 kHz cut off frequency. At this stage, an augmented PID controller was designed where second order lead-lag compensators are used to damped high frequency modes. The position of the rotor as well as its time derivatives and integrals are inputs of their related gain. The controller characteristics are adapted to bring damping and stiffness in the operating speed range but also on the modes above this range to avoid any spillover effects.

The numerical model is now completely described. In the next part, the effect of the base motion combined with the mass unbalance, the gravity and the control on the rotor response is analyzed.

### 3.2 Numerical results

Rotating machinery supported by AMB can be subjected to different base motions implying sometimes high vibration amplitudes. An augmented PID was designed for classical rotor dynamics purpose. AMBs are not specifically tuned for base motion purpose. The objective is to analyze the capability of a classical augmented PID to sustain a rotor subject to gravity forces, mass unbalance forces and base motion effects. The imposed base motions are harmonic rotations (pitching and rolling), earthquake and shock. The mass unbalance is determined according to API 617 standards and located on the disk. The magnetic forces  $f_{amb}$  and the nodal equivalent forces  $f_{gravity}$  due to gravity are added to the EoM in Eq. 3, solved with the 5<sup>th</sup> Runge-Kutta scheme with a variable time step. The base motion is introduced after 1s of simulation, when the steady-state harmonic response of the shaft is reached. The rotor is initially located at the bottom of its TDB then the integral gain centers it. The rotor deflections are observed at the sensors locations. Only the harmonic pitching motion and the earthquake cases are detailed, the rotor lateral maximal deflections are reported in Table 3 for the other cases. All tests were performed at 9 500 rpm.

The harmonic pitching motion, as tested section 2, is imposed to the base. The rotor deflections, Fig. 6, do not consumed the TDB clearance (black circle) and do not create particular instabilities. Quite no lateral coupling effects are exhibited since gyroscopic effects are weak. Lateral deflections are smaller and quasi-periodic orbits are found unlike the orbit plotted Fig. 3. This is due to the fact that the rotor rotational speed and the harmonic pitching frequency of the base are not related by any mathematical relationship, as shown in (Driot et al. 2006). The linear assumption of the AMB remains valid (small displacements) and the control currents at both driving end (DE) and NDE remain in the operating range.

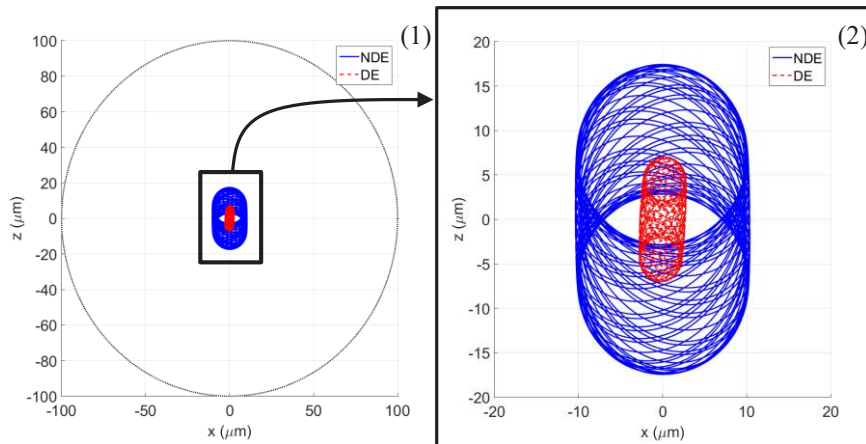


Fig. 6. Rotor orbits at DE and NDE (1) and zoom (2)

Emergency steam turbines in nuclear plants have to withstand seisms. The rotor is subjected to the El Centro earthquake that hit the Imperial Valley in California with a magnitude of 7.1 in 1940. The north-south (NS) waves generated the highest energy and are imposed to the base in the horizontal direction. The time history data file comes from the Pacific Earthquake Engineering Research Center.

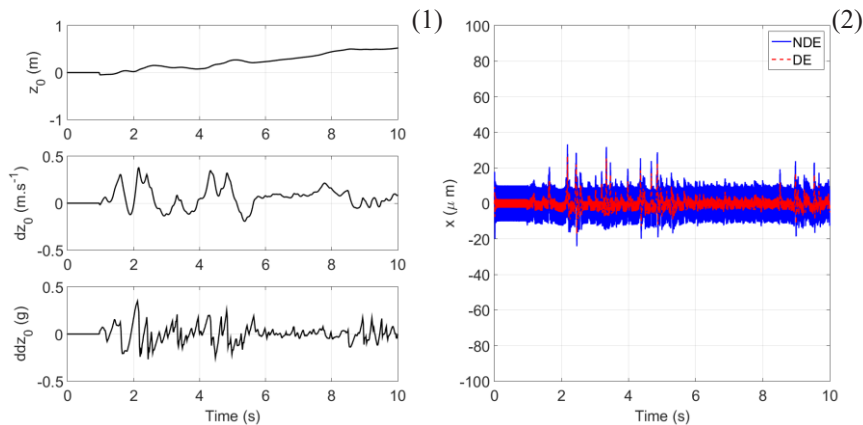


Fig. 7. NS waves (1) and rotor response at DE and NDE sensors (2)

Orbit plots are not presented here since quite no displacements were noticed in z-direction due to the lack of gyroscopic effects. The predicted horizontal deflections, Fig. 7, do not consumed the TDB clearance and do not create particular instabilities. The highest deflections are related to the highest level of acceleration. As for the previous case, the assumptions concerning the AMBs remain valid.

Compressors on FPSO (Floating production storage and offloading) are subjected to ocean excitations like shock due to impact waves or harmonic rolling motion due to surface gravity waves. Here, the shock was modeled with a 3g half-sine according to (Lee et al. 2006) and the harmonic rolling motion was a sine wave of 0.1 Hz and an amplitude of  $\pm 60^\circ$ , according to standards. Results reported in Table 3 represent the maximal rotor deflections subject to the different base motions tested in this work. The crossed box represents the case where no base motions are imposed.

Table 3. Maximal rotor deflections depending on the base motion type

Base motion type	DE [ $\mu\text{m}$ ]	NDE [ $\mu\text{m}$ ]
<del> </del>	2.5	10
Harmonic rotation (Driot et al. 2006)	7	17
Earthquake – El Centro	27	33
Rolling motion	2.5	10
Half-sine shock (Lee et al. 2006)	Contact with TDB	Contact with TDB

## Conclusion

The dynamic behavior of a rotor suspended by AMB and subject to gravity, unbalance forces and rigid base motions was investigated. First, the FE modelling is used to establish the matrices and external force vectors involved in the equations of motion. The developed model was validated with previous experimentations where rotor was supported on classical ball-bearings. Then, the augmented PID controller designed for classical rotor dynamics purpose was implemented in the model. It is shown that this controller is able to sustain satisfactorily the AMB-rotor system subject to the El-Centro earthquake and to the imposed harmonic pitching motion even if undesirable vibrations remain. Rolling motions due to surface gravity waves have no effect on the rotor dynamics due to their very low frequencies. The 3g half-sine shock led to contact with TDB and current saturations occurred. A best control strategy is required to reduce the vibration amplitudes related to the rigid base motions without deteriorating the vibration control related to unbalance. This control strategy should be able to limit either harmonic or transient base motions. The used PID could be improved for this purpose and / or another control loop (feedback, feedforward...) could be added.

## Acknowledgments

This work is a part of Clément JARROUX PhD performed with the support of CIFRE funding N0 2013/1376. The authors are grateful to the ANRT National Agency.

## References

- Cole MOT, Keogh PS, and Burrows CR. 1998. Vibration control of a flexible rotor/magnetic bearing system subject to direct forcing and base motion disturbances. *Proceedings of the Institution of Mechanical Engineers, Part C: Journal of Mechanical Engineering Science* 212(7):535-546.
- Dakel M, Baguet S, and Dufour R. 2014a. Nonlinear dynamics of a support-excited flexible rotor with hydrodynamic journal bearings. *Journal of Sound and Vibration* 333(10):2774-2799.
- Dakel M, Baguet S, and Dufour R. 2014b. Steady-state dynamic behavior of an on-board rotor under combined base motions. *Journal of Vibration and Control* 20(15):2254-2287.
- Das AS, Dutt JK, and Ray K. 2010. Active vibration control of unbalanced flexible rotor-shaft systems parametrically excited due to base motion. *Applied Mathematical Modelling* 34(9):2353-2369.
- Defoy B, Alban T, and Mahfoud J. 2014. Experimental Assessment of a New Fuzzy Controller Applied to a Flexible Rotor Supported by Active Magnetic Bearings. *Journal of Vibration and Acoustics* 136(5):051006-051006.
- Defoy B, Alban T, and Mahfoud J. 2015. Energy cost assessment of a polar based controller applied to a flexible rotor supported by AMB. *Mechanical Engineering Journal*.
- Driot N, Lamarque CH, and Berlioz A. 2006. Theoretical and Experimental Analysis of a Base-Excited Rotor. *Journal of Computational and Nonlinear Dynamics* 1:257-263.
- Duchemin M. 2003. Contribution à l'étude du comportement dynamique d'un rotor embarqué. Lyon: INSA de Lyon.
- Duchemin M, Berlioz A, and Ferraris G. 2006. Dynamic Behavior and Stability of a Rotor Under Base Excitation. *Journal of Vibration and Acoustics* 128(5):576-585.
- Han Q, and Chu F. 2015. Parametric instability of flexible rotor-bearing system under time-periodic base angular motions. *Applied Mathematical Modelling* 39(15):4511-4522.
- Kasarda ME, Clements J, Wicks AL, Hall CD, and Kirk RG. 2000. Effect of sinusoidal base motion on a magnetic bearing. *Control Applications, 2000 Proceedings of the 2000 IEEE International Conference on*. p 144-149.
- Keogh PS, Sahinkaya MN, Burrows CR, and Prabhakar S. 2006. Wavelet Based Adaptation of H-infinity Control in Flexible Rotor/Magnetic Bearing Systems. 7th IFToMM Conference on Rotor dynamics. Vienne.
- Lee AS, Kim BO, and Kim Y-C. 2006. A finite element transient response analysis method of a rotor-bearing system to base shock excitations using the state-space Newmark scheme and comparisons with experiments. *Journal of Sound and Vibration* 297(3-5):595-615.
- Marx S, and Nataraj C. 2007. Suppression of Base Excitation of Rotors on Magnetic Bearings. *International Journal of Rotating Machinery* 2007:10.
- Matsushita O, Imashima T, Hisanaga Y, and Okubo H. 2001. Aseismic Vibration Control of Flexible Rotors Using Active Magnetic Bearing. *Journal of Vibration and Acoustics* 124(1):49-57.
- Murai Y, Watanabe K, and Kanemitsu Y. 1989. Seismic Test on Turbo-Molecular Pumps Levitated by Active Magnetic Bearing. In: Schweitzer G, editor. *Magnetic Bearings: Proceedings of the First International Symposium, ETH Zurich, Switzerland, June 6-8, 1988*. Berlin, Heidelberg: Springer Berlin Heidelberg. p 303-310.
- Suzuki Y. 1998. Acceleration feedforward control for active magnetic bearing systems excited by ground motion. *IEE Proceedings - Control Theory and Applications* 145(2):113-118.